Magnetic-field-inspired Navigation for Soft Continuum Manipulator*

A. Ataka[1,2], A. Shiva[1], H.K. Lam[1], and K. Althoefer[2]

Abstract— **Taking inspiration from the properties of magnetic fields, we propose a reactive navigation method for soft continuum manipulators operating in unknown environments. The proposed navigation method outperforms previous works since it is able to successfully achieve collision-free movements towards the goal in environments with convex obstacles without relying on a priori information of the obstacles' shapes and locations. Simulations for the kinematic model of a soft continuum manipulator and preliminary experiments with a 2-segments soft continuum arm are performed, showing promising results and the potential for our approach to be applied widely.**

I. INTRODUCTION

In the last decade, inspiration from species in nature such as the octopus has sparked a new trend in robotics aiming to improve robotic dexterity and manoeuvrability beyond what is possible with existing rigid link manipulators. This has given birth to a new breed of robots - robots that are characterized by a soft, continuum structure such as the pneumatically actuated robotic arms [1], tendon-driven manipulators [2], or combination of tendon and pressure actuation to manoeuvre and, at the same time, control the stiffness of the mechanical structure [3]. Although this development shows encouraging improvement in terms of the robot's flexibility, opening the door for applications which were not possible beforehand, it also creates new challenges in terms of robot modelling, control, and navigation due to the nonlinear behaviour of the soft mechanical structure employed.

As the robot application starts to extend beyond the well-defined environments of industrial settings, the subject of robot navigation continues to be an on-going focus of various works. However, research which focuses on navigating the continuum manipulator in an unknown environment is still in its early stages. Most of the previous works employed optimization-based planning [4]-[5] or sampling-based planning [6]-[7]. These methods assume to have (at least) near-complete knowledge of the environment prior to initiating any robot movement. The same drawback occurs for recent works employing neural dynamics approach [8], while the effort to use supervised learning by demonstration [9] needs the intervention of human to generate the training data. Some other studies which try to tackle dynamic environments are mainly constrained to specific geometries and/or applications. An adaptive motion planning, used to navigate the OctArm manipulator in [10], needs the knowledge of obstacle's geometry and is limited to planar scenarios.

Taking inspiration from natural physical phenomena is also useful in robot navigation. Examples include the electric potential field which took the idea of electrostatic interaction among charged particles forming the basis for robot obstacle avoidance and goal tracking [11]. Being relatively simple, this method has been extensively applied in various robotics systems, including mobile robots and rigid-link manipulators [11]. Recent work exploring the application of the electric potential field for continuum manipulators has been reported in [12]. However, the global convergence is not guaranteed in this algorithm. Other inspirations from nature applied the properties of an artificial magnetic field for navigating rigid-link manipulators, such as reported in [13]-[14], claiming to resolve the problem of entrapment in local minima observed when using the electric potential field method. These methods, though, requires the geometry and location of any obstacle or its centre point to be known beforehand.

In this paper, we present a reactive navigation algorithm for soft continuum manipulator which is inspired by the characteristics of magnetic fields. The algorithm is reactive in the sense that it only relies on the most-recent sensory information to navigate the environment without the need for prior knowledge of the obstacles' position or geometrical properties. The backbone of the manipulator is considered as a means for a virtual current flow, resembling an electrical wire which induces an artificial electrical current on nearby objects. The artificial current will then produce a magnetic field which will impact on the continuum manipulator movements avoiding a collision. To the best of our knowledge, this is the first work which takes inspiration from nature to navigate soft continuum manipulators in unknown environments.

II. INSPIRATION FROM NATURE

A wire segment of an infinitesimal length $\mathbf{dl}_o$ with electrical current i_o as illustrated in Fig. 1a produces an infinitesimally small magnetic field $\mathbf{dB}$ as follows [15]

$$\mathbf{dB} = \frac{\mu_0}{4\pi} \frac{i_o \mathbf{dl}_o \times \mathbf{r}}{|\mathbf{r}|^3}, \tag{1}$$

in which $\mathbf{r}$ stands the position vector of a point with respect to the wire, μ_0 is a permeability constant, and $\times$ denotes the cross product operation. This magnetic field produces a force

*This work was supported in part by King's College London, the EPSRC in the framework of the NCNR (National Centre for Nuclear Robotics) project (EP/R02572X/1), the STIFF-FLOP project grant from the European Communities Seventh Framework Programme under grant agreement 287728, and the Indonesia Endowment Fund for Education, Ministry of Finance Republic of Indonesia.

[1]A. Ataka, A. Shiva, and H.K. Lam are with The Centre for Robotics Research (CoRe), Department of Informatics, Kings College London, London WC2R 2LS, United Kingdom.

[2]A. Ataka and K. Althoefer are with the Centre for Advanced Robotics @ Queen Mary (ARQ), Faculty of Science and Engineering, Queen Mary University of London, Mile End Road, London E1 4NS, United Kingdom.

Corresponding author e-mail: ahmad.ataka@kcl.ac.uk

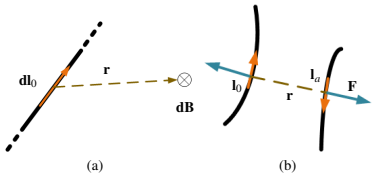

Fig. 1. (a) An electric current induces a magnetic field **dB** which, in this figure, points inside towards the paper. (b) Two current-carrying wires with currents flow opposite to each other, $\mathbf{l}_a$ and $\mathbf{l}_o$, produce repulsion force $\mathbf{F}$.

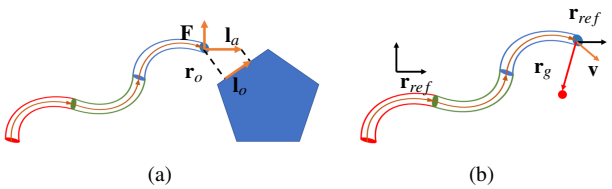

Fig. 2. (a) The tip of the continuum manipulator induces an artificial current $\mathbf{l}_o$ on the obstacle as a projection of its velocity direction $\mathbf{l}_a$, producing force $\mathbf{F}$ as a result. (b) The tip navigation employs the transformation of the robot's velocity $\mathbf{v}$ and tip-to-goal $\mathbf{r}_g$ with respect to reference vector $\mathbf{r}_{ref}$.

$\mathbf{dF}$ on another current-carrying wire with an infinitesimal length $\mathbf{dl}_a$ and current i_a, as illustrated in Fig. 1b, given by

$$\mathbf{dF} = i_a \mathbf{dl}_a \times \mathbf{B}. \tag{2}$$

The magnetic field also influences a moving particle with electrical charge dq and velocity $\mathbf{v}$ by a force given by

$$\mathbf{dF} = dq \ \ \mathbf{v} \times \mathbf{B}. \tag{3}$$

Substituting (1) to (2) and dropping all the infinitesimal notation, we can then derive the force interaction between two current-carrying wires as follows

$$\mathbf{F} = \frac{\mu_0 i_a i_o}{4\pi} \ \ \frac{\mathbf{l}_a \times (\mathbf{l}_o \times \mathbf{r})}{|\mathbf{r}|^3}. \tag{4}$$

Inspired by this physical phenomenon, we can see a soft continuum manipulator as a current-carrying wire with current direction $\mathbf{l}_a$, either "flowing" on the tip or the body of manipulator, inducing an artificial current $\mathbf{l}_o$ on the obstacle surface located at position $\mathbf{r}_o$ with respect to the manipulator. This current induced on the obstacle will produce magnetic field $\mathbf{B}$ which will produce a force on the robot current in such a way that the force $\mathbf{F}$ will guide the robot away from the obstacle. It is noted that $\mathbf{r}_o = -\mathbf{r}$, so that equation (4) can be rewritten in a more general form as follows

$$\mathbf{F}(\mathbf{r}_o) = c \ \ \mathbf{l}_a \times (\mathbf{r}_o \times \mathbf{l}_o) \ \ f(|\mathbf{r}_o|), \tag{5}$$

where $c > 0$ is a scalar constant and $f(|\mathbf{r}_o|) \geq 0$ is a positive scalar function. For simplification, a skew-symmetric matrix $\hat{\mathbf{l}}$ is used to replace the vector cross product operation $\mathbf{l}\times$ of a vector $\mathbf{l} = \begin{bmatrix} l_x & l_y & l_z \end{bmatrix}^T$ and defined as follows

$$\hat{\mathbf{l}} = \begin{bmatrix} 0 & -l_z & l_y \\ l_z & 0 & -l_x \\ -l_y & l_x & 0 \end{bmatrix}. \tag{6}$$

III. NAVIGATION ALGORITHM

A. Tip Navigation

When moving closer to the surface of an obstacle, the tip of the robot located at location $\mathbf{p}$ will induce an artificial electric current $\mathbf{l}_o$ on the obstacle surface as follows

$$\mathbf{l}_o = \mathbf{l}_a - \frac{(\mathbf{l}_a^T \mathbf{r}_o)\mathbf{r}_o}{|\mathbf{r}_o|^2}, \tag{7}$$

where $\mathbf{l}_a$ and $\mathbf{r}_o$ stand for a unit vector in the direction of the tip's velocity and the position of the closest obstacle point with respect to the robot's tip, respectively. Eq. (7) ensures that the artificial current $\mathbf{l}_o$ is a projection of the tip's velocity $\dot{\mathbf{p}}$ (whose direction is described by a unit vector $\mathbf{l}_a$) on to the obstacle surface as depicted in Fig. 2a.

To make sure that the robot's tip changes its motion direction towards the direction of artificial current $\mathbf{l}_o$, the vector field $\mathbf{F}$ in (5) is modified as follows

$$\mathbf{F} = c \ \ \mathbf{l}_a \times (\mathbf{l}_o \times \mathbf{l}_a) \ \ f(|\mathbf{r}_o|, |\dot{\mathbf{p}}|). \tag{8}$$

To make sure that the tip does not touch the obstacle, the scalar function $f(|\mathbf{r}_o|, |\dot{\mathbf{p}}|)$ is designed to be proportional to the tip's velocity $v = |\dot{\mathbf{p}}|$ and inversely proportional to the distance towards the obstacle surface $r = |\mathbf{r}_o|$ when the tip is closer to the obstacle than a limit distance r_l as follows

$$f(|\mathbf{r}_o|, |\dot{\mathbf{p}}|) = \begin{cases} \frac{v}{r} & \text{if } r < r_l \\ 0 & \text{if } r \geq r_l \end{cases}. \tag{9}$$

Using the formulation described in eq. (7)-(9), the vector field $\mathbf{F}$ has several properties (which were thoroughly described in our previous works [16],[17]) as follows:

1) Zero work: The vector field $\mathbf{F}$ does not have a component in the direction of the tip's velocity $\mathbf{l}_a$, leaves the robot's speed unchanged, and hence, it does not change the energy of the system. Combined with a globally-stable goal attraction, the vector field $\mathbf{F}$ does not create local minima.

2) Obstacle Boundary Following: Considering that the tip's direction $\mathbf{l}_a$ is not in line with the position of the obstacle $\mathbf{r}_o$, the vector field $\mathbf{F}$ will always have a component along the direction of the artificial current $\mathbf{l}_o$ and will force the tip to follow the obstacle's boundary.

3) Collision Avoidance: The scalar function in (9) guarantees that the tip will avoid touching the surface of a convex-shaped obstacle, as long as its movement direction $\mathbf{l}_a$ is not in line with the position of the obstacle $\mathbf{r}_o$.

In reality, we want the tip to not only avoid collision with an obstacle's surface but also to be at a safe distance from the surface. To ensure this, we add an avoidance term inspired by the behaviour of a pair of current-carrying wires (see Fig. 1b). The tip of the continuum robot will induce an artificial current $\mathbf{l}_{o\perp}$ in the opposite direction of current $\mathbf{l}_o$ in (7). The avoidance term $\mathbf{F_a}$ can then be derived following the general equation in (5) with the scalar function $f(|\mathbf{r}_o|)$ being chosen to be inversely proportional to the square of robot-obstacle distance r as follows

$$\mathbf{F_a} = \mathbf{l}_a \times (\frac{\mathbf{r}_o}{r} \times \mathbf{l}_{o\perp}) \ \ f(|\mathbf{r}_o|), \tag{10}$$

$$f(|\mathbf{r}_o|) = \begin{cases} c_\perp(\frac{1}{r} - \frac{1}{r_b})\frac{1}{r^2} & \text{if } r < r_b \\ 0 & \text{if } r \geq r_b \end{cases}, \tag{11}$$

where $c_\perp$ denotes a positive constant and $r_b < r_l$ denotes a limit distance. Similar to vector field $\mathbf{F}$ in (8), the avoidance field $\mathbf{F_a}$ also does no work (i.e. $\mathbf{l}_a^T \mathbf{F_a} = 0$). The avoidance term in (10)-(11) will make sure that the tip is repelled from the obstacle when it is too close without affecting its speed. The overall avoidance vector field can then be written as

$$\mathbf{F}_o = \mathbf{F} + \mathbf{F_a}. \tag{12}$$

To guide the tip of the continuum manipulator to a desired position $\mathbf{p_g}$, a PD controller can be employed as follows

$$\mathbf{F}_{pd} = -K_P(\mathbf{p} - \mathbf{p_g}) - K_D\dot{\mathbf{p}}, \tag{13}$$

where K_P and K_D are positive constants. However, when the tip is located at a considerable distance from the goal, this approach could force the tip to move at high speeds, leading to an exorbitantly high avoidance term $\mathbf{F}_o$ which may not be achievable by the robot's actuators when avoiding obstacles.

An alternative way to guide the tip towards the goal is by implementing a geometric control term, originally presented in [18]. We assume here that the tip of the continuum robot moves with velocity $\mathbf{v}$ as depicted in Fig. 2b. With respect to a static unit reference vector $\mathbf{r}_{ref}$, vector $\mathbf{v}$ is expressed as a rotation matrix $\mathbf{R}_v$ as follows

$$\mathbf{R}_v = \mathbf{I} + \hat{\omega}_v + \hat{\omega}_v^2 \frac{1}{1 + \cos\phi}, \tag{14}$$

where $\omega_v = \hat{\mathbf{r}}_{ref}\frac{\mathbf{v}}{|\mathbf{v}|}$, $\cos\phi = \mathbf{r}_{ref}^T\frac{\mathbf{v}}{|\mathbf{v}|}$, and $\mathbf{I} \in \mathbb{R}^{3\times3}$ stands for the 3×3 identity matrix. Applying the same approach for "tip-to-goal" vector $\mathbf{r}_g = \mathbf{p_g} - \mathbf{p}$, we can obtain its orientation $\mathbf{R}_g$ with respect to $\mathbf{r}_{ref}$. We aim to move the tip of the robot from orientation $\mathbf{R}_v$ to orientation $\mathbf{R}_g$ by introducing an error matrix $\mathbf{R}_e = \mathbf{R}_g^T\mathbf{R}_v$ and applying a control law as follows

$$\hat{\omega}_g = -K_\omega \log(\mathbf{R}_e), \tag{15}$$

in which $K_\omega \geq 0$ stands for a constant and the operator $\log(\mathbf{R})$ for any $\mathbf{R} \in SO(3)$ is defined as $\log(\mathbf{R}) = \frac{\beta}{2\sin\beta}(\mathbf{R} - \mathbf{R}^T)$ where $\beta = \arccos(\frac{tr(\mathbf{R})-1}{2})$. Using the definition of a skew-symmetric matrix in (6), we get the angular speed $\omega_g \in \mathbb{R}^3$ from $\hat{\omega}_g$. To express the angular speed in the static frame of $\mathbf{r}_{ref}$, we do matrix transformation $\omega_{ref} = \mathbf{R}_g\omega_g$. Finally, the vector field to produce this angular speed is

$$\mathbf{F}_{gc} = \hat{\omega}_{ref}\mathbf{v}. \tag{16}$$

The vector field $\mathbf{F}_{gc}$ guides the robot towards the direction of the goal without changing its speed. Hence, to make the robot starts moving, we add a speed controller as follows

$$\mathbf{F}_v = -K_v(v - v_d)\mathbf{d}, \tag{17}$$

where $K_v > 0$ stands for a positive constant, v_d is a desired speed of the tip, and $\mathbf{d}$ is defined as $\mathbf{d} = \begin{cases} \frac{\mathbf{r}_g}{|\mathbf{r}_g|} & \text{if } |\mathbf{v}| = 0 \\ \frac{\mathbf{v}}{v} & \text{if } |\mathbf{v}| > 0 \end{cases}$. Finally, when the robot is closer to the goal than a limit distance r_{gl}, we then switch back to the PD controller in (13) to make the robot asymptotically reach the goal in a smooth fashion. Hence, the overall vector field guiding the tip's movement is given by

$$\mathbf{F}_t = \begin{cases} \mathbf{F}_o + \mathbf{F}_{gc} + \mathbf{F}_v & \text{if } |\mathbf{r}_g| \geq r_{gl} \\ \mathbf{F}_o + \mathbf{F}_{pd} & \text{if } |\mathbf{r}_g| < r_{gl} \end{cases}. \tag{18}$$

B. Whole Body Collision Avoidance

Besides the tip, we also apply the magnetic-field-inspired vector field to the part of the robot's structure which is closest to the nearby obstacles. We choose m uniformly-distributed points along the longitudinal axis of the manipulator which are subjected to the vector field. Vector field $\mathbf{F_b}$ will be applied to the point which is closest to the nearby obstacle. For simplicity, we call this point *active point* located at $\mathbf{p}_a$.

Since the body of the manipulator does not have to reach a certain configuration, the only vector field which we need is the avoidance term in (12). Since there is no need for the active point to have a constant speed, we modify the vector field $\mathbf{F_a}$ in (10) to simply be a repulsive field $\mathbf{F_b} = \frac{\mathbf{r}_o}{r}\ f(|\mathbf{r}_o|)$, where $r = |\mathbf{r}_o|$ stands for the distance from the active point on the manipulator body towards the closest obstacle point.

For the active point, the boundary-following vector field $\mathbf{F}$ in (8) needs to be used only for a certain condition, i.e. when at least 2 of the 3 conditions below are satisfied:

1) The active point is occluded by the obstacle from the goal position $\mathbf{p_g}$,
2) The artificial current $\mathbf{l}_o$ induced by the active point does not tend to attract the point towards a direction opposite to the goal,
3) The tip has not reached goal location $\mathbf{p_g}$.

Apart from these, the vector field $\mathbf{F}$ could create unnecessary movements to the manipulator's body. To implement these 3 conditions, we introduce 3 weights w_a, w_b, w_c as follows

$$\begin{aligned} w_a &= \begin{cases} 0 & \text{if } \cos\alpha < 0 \\ 1 & \text{if } \cos\alpha \geq 0 \end{cases}, \\ w_b &= \begin{cases} 0 & \text{if } \cos\gamma < 0 \\ 1 & \text{if } \cos\gamma \geq 0 \end{cases}, \\ w_c &= \begin{cases} 0 & \text{if } |\mathbf{p} - \mathbf{p_g}| < r_l \\ 1 & \text{if } |\mathbf{p} - \mathbf{p_g}| \geq r_l \end{cases}, \end{aligned} \tag{19}$$

where α stands for the angle between vector $\mathbf{r}_{ag} = \mathbf{p_g} - \mathbf{p}_a$ and body-to-obstacle vector $\mathbf{r}_o$, while γ stands for the angle between vector $\mathbf{r}_{ag}$ and artificial current induced by active point $\mathbf{l}_o$. Whenever (at least) 2 of these 3 weights are 1, then the overall weight w_{tot} will be 1, and otherwise will be zero. Eq. (12) for the active point is then modified into

$$\mathbf{F}_{ob} = w_{tot}\mathbf{F} + \mathbf{F_b}. \tag{20}$$

IV. IMPLEMENTATION

The proposed methods were implemented on a kinematic model of multi-segment continuum manipulator. A modal kinematic approach, using 11th order multivariate Taylor series expansion as presented in [19], is used to model the

shape of each segment. Hence, segment i can be described by a set of actuator space variables $\mathbf{q}_i = \begin{bmatrix} l_{i1} & l_{i2} & l_{i3} \end{bmatrix}^T$ where $L_0 + l_{ij}$ represents the length of tendon j in segment i for an initial length L_0. For manipulator with static base, the overall actuator space variables for N segments manipulator can then be written as $\mathbf{q} = \begin{bmatrix} \mathbf{q}_1 & \mathbf{q}_2 & \dots & \mathbf{q}_N \end{bmatrix}^T$, whereas for manipulator with movable base we have $\mathbf{q} = \begin{bmatrix} \mathbf{q}_0 & \mathbf{q}_1 & \dots & \mathbf{q}_N \end{bmatrix}^T$ where $\mathbf{q}_0 \in \mathbb{R}^2$ represents the base's position. Any point along the body of segment i can be described with respect to the base of segment i using modal homogeneous transformation matrix ${}^{i}_{i-1}\mathbf{T}(\mathbf{q}_i, \xi_i) \in SE(3)$. A scalar $\xi_i \in [0,1]$ corresponds with the location of the corresponding point along the backbone of segment i. To describe the pose of any point along the body of multi-segment manipulator with respect to the base, the complete homogeneous matrix for N segments manipulator can be derived as follows

$$ {}^{N}_{0}\mathbf{T}(\mathbf{q}, \xi) = \prod_{i=1}^{N} {}^{i}_{i-1}\mathbf{T}(\mathbf{q}_i, \xi_i) = \begin{bmatrix} \mathbf{R}(\mathbf{q}, \xi) & \mathbf{p}(\mathbf{q}, \xi) \\ \mathbf{0} & 1 \end{bmatrix}, \quad (21) $$

where $\mathbf{R}(\mathbf{q}, \xi) \in SO(3)$ and $\mathbf{p}(\mathbf{q}, \xi) \in \mathbb{R}^3$ stand for rotation matrix and position vector of the corresponding point. A Jacobian, $\mathbf{J}(\mathbf{q}, \xi) \in \mathbb{R}^{3\times(3N)}$ for a static base or $\mathbf{J}(\mathbf{q}, \xi) \in \mathbb{R}^{3\times(3N+2)}$ for a planar mobile base, relating the velocity vector in the joint space to the task space, can be derived via numerical computation given by $[\mathbf{J}]_{kl} = \frac{[\mathbf{p}]_k([\mathbf{q}]_l + \delta, \xi) - [\mathbf{p}]_k([\mathbf{q}]_l, \xi)}{\delta}$, where $[\mathbf{J}]_{kl}$ stands for the component of a Jacobian matrix in row-k and column-l, $[\mathbf{p}]_k$ stands for the component of vector $\mathbf{p}$ in row-k, and δ stands for small positive constant.

Since we consider only the kinematics of the system, force $\mathbf{F}$ computed using the proposed method needs to be numerically integrated to produce a task-space velocity $\dot{\mathbf{p}}$ given by $\dot{\mathbf{p}}(t + \Delta t) = \dot{\mathbf{p}}(t) + \mathbf{F}(t)\Delta t$. This equation is used to produce the task-space tip velocity $\dot{\mathbf{p}}_t$ and body velocity $\dot{\mathbf{p}}_b$ from the vector field $\mathbf{F}_t$ in (18) and $\mathbf{F}_{ob}$ in (20) respectively.

To convert this joint-space velocity $\dot{\mathbf{p}}$ to the actuator space velocity $\dot{\mathbf{q}}$, assuming the segment number $N \geq 3$, we exploit the redundancy of the continuum manipulator in order to implement several tasks according to priority list as follows:

1) Tip navigation,
2) Whole body obstacle avoidance,
3) Actuator space constraint avoidance.

When the part of the manipulator's body is close to the obstacle, the actuator space velocity consists of 3 terms [20]:

$$ \begin{aligned} \dot{\mathbf{q}} &= \dot{\mathbf{q}}_t + \dot{\mathbf{q}}_b + \dot{\mathbf{q}}_{c1}, \\ \dot{\mathbf{q}}_t &= \mathbf{J}_t^{+} \dot{\mathbf{p}}_t, \\ \dot{\mathbf{q}}_b &= \lambda_b (\mathbf{J}_b (\mathbf{I} - \mathbf{J}_t^{+} \mathbf{J}_t))^{+} (\dot{\mathbf{p}}_b - \mathbf{J}_b \mathbf{J}_t^{+} \dot{\mathbf{p}}_t), \\ \dot{\mathbf{q}}_{c1} &= \lambda_{c1} (\mathbf{I} - \mathbf{J}_t^{+} \mathbf{J}_t)(\mathbf{I} - \tilde{\mathbf{J}}^{+} \tilde{\mathbf{J}}) \mathbf{z} \end{aligned} \quad (22) $$

where $^{+}$ denotes pseudo-inverse operation defined as $\mathbf{J}^{+} = \mathbf{J}^T (\mathbf{J}\mathbf{J}^T)^{-1}$, $\mathbf{J}_t$ and $\mathbf{J}_b$ stand for the Jacobian of the tip and the active point on the manipulator's body respectively, λ_b and λ_{c1} stand for positive constants, while $\tilde{\mathbf{J}} = \mathbf{J}_b (\mathbf{I} - \mathbf{J}_t^{+} \mathbf{J}_t)$ and $\mathbf{z} \in \mathbb{R}^{3N}$ or $\mathbf{z} \in \mathbb{R}^{3N+2}$ (depending whether the base is fixed or mobile) stands for arbitrary vector. When the part of the manipulator's body is far from the obstacle, the actuator space velocity consists of only 2 terms, namely the tip navigation and constraint avoidance as follows

$$ \begin{aligned} \dot{\mathbf{q}} &= \dot{\mathbf{q}}_t + \dot{\mathbf{q}}_{c2}, \\ \dot{\mathbf{q}}_t &= \mathbf{J}_t^{+} \dot{\mathbf{p}}_t, \\ \dot{\mathbf{q}}_{c2} &= \lambda_{c2} (\mathbf{I} - \mathbf{J}_t^{+} \mathbf{J}_t) \mathbf{z}, \end{aligned} \quad (23) $$

where λ_{c2} is a positive constant. To ensure smooth transition of (22) and (23), the actuator space velocity is given by

$$ \dot{\mathbf{q}} = \dot{\mathbf{q}}_t + \dot{\mathbf{q}}_b + \dot{\mathbf{q}}_{c1} + \dot{\mathbf{q}}_{c2}, \quad (24) $$

while the positive constants λ_b, λ_{c1}, and λ_{c2} are defined as

$$ \begin{aligned} \lambda_b &= \begin{cases} 0 & \text{if } r \geq r_{l2} \\ \cos^2\left(\frac{\pi}{2} \frac{r - r_{l1}}{r_{l2} - r_{l1}}\right) & \text{if } r \geq r_{l1} \text{ and } r < r_{l2} \\ 1 & \text{if } r < r_{l1} \end{cases}, \\ \lambda_{c1} &= \lambda_b, \lambda_{c2} = 1 - \lambda_{c1}, \end{aligned} \quad (25) $$

where r_{l1} and r_{l2} specify limit distances.

To minimize the possibility of the actuators reaching their limit (i.e. minimum length l_{min} or maximum length l_{max}), the vector $\mathbf{z}$ is designed to attract the length of the tendon to its middle length $l_{mid} = l_{min} + \frac{l_{max} - l_{min}}{2}$. Vector $\mathbf{z}$ is numerically integrated from its rate $\dot{\mathbf{z}}$ given by $\dot{\mathbf{z}} = (-\frac{K_{Pz}}{(l_{mid} - l_{min})^2}(\mathbf{q} - l_{mid}\mathbf{I}) - K_{Dz}\dot{\mathbf{q}})$, for the case of a fixed base. For the mobile base, the vector $\mathbf{z}$ is added to vector $\mathbf{z}_0$, which attracts the base to the projection of the tip position into the xy plane $\mathbf{p}_{xy}$, whose rate is given by $\dot{\mathbf{z}}_0 = (-\frac{K_{Pz0}}{(l_{mid} - l_{min})^2}(\mathbf{q}_0 - \mathbf{p}_{xy}) - K_{Dz}\dot{\mathbf{q}}_0)$. To further reduce the probability of the manipulator's actuator reaching its maximum length, the artificial current in (7) for the tip navigation is projected into the xy plane if the z component is positive. For the active point on the manipulator's body, the induced artificial current is projected into the xy plane straightaway.

Finally, the actuator space velocity in (24) is integrated to get the actuator space variables (i.e. the chamber length l_{ij}) and transformed into a pressure value for actuation by equation $p_{ij} = \frac{EA_w}{AL_0} l_{ij}$, where E, A_w, and A stand for Young modulus, cross-sectional area of a segment, and cross sectional area of each chamber in every segment respectively.

V. RESULTS AND ANALYSIS

In this section, we evaluate the performance of the algorithm in the simulation and preliminary experimental scenario. Static obstacles with varying dimension and position are placed in the vicinity of the manipulator. It is noted that the manipulator is only able to detect the obstacle when the distance to the closest obstacle is less than r_{l2}. We compare the performance of the proposed algorithm with previous electric-field-based navigation as described in [12]. All the codes are implemented via the Robot Operating System (ROS) framework. A video attachment is also available.

A. Simulation Results

In the simulation scenario, the model of a three-segment continuum manipulator was used. Three points per segment, distributed uniformly along the backbone of each segment,

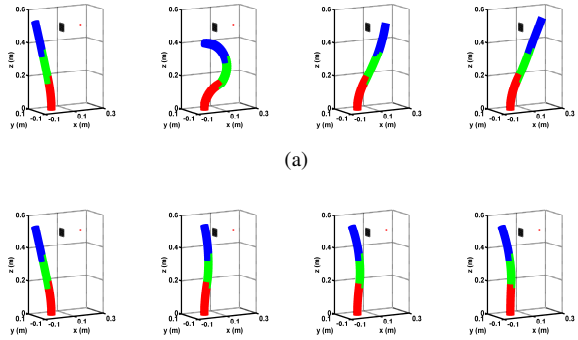

(a) (b)

Fig. 3. The scenario where the 3-segments continuum manipulator is located in an environment consisting of a planar obstacle (black), using (a) magnetic-field-inspired and (b) artificial potential field algorithms. The subpictures are to be viewed from left to right.

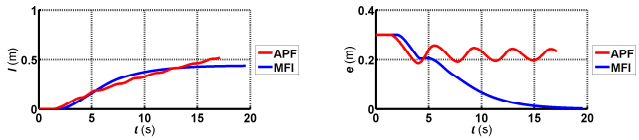

(a) (b)

Fig. 4. The plot of (a) the tip trajectory and (b) the position error for a planar obstacle for magnetic-field-inspired navigation (blue) and artificial potential field (red).

are chosen to be the active points. We evaluate two cases: one where the robot has a static base and one where the robot is situated on a mobile base operating in a planar environment.

We first test the scenario where the environment consists of a planar obstacle as shown in Fig. 3. In Fig. 3a, we can see how the magnetic-field-inspired (MFI) navigation algorithm guides the tip of the continuum manipulator towards the goal shown as a red dot without colliding with the planar obstacle. In contrast, the artificial potential field (APF) in Fig. 3b fails to guide the tip of the continuum manipulator towards the desired target since the attractive field to the goal is cancelled by the repulsive field from the planar obstacle, resulting in an entrapment in a local minimum.

In Fig. 4, we can see how the two algorithms are compared in terms of their tip's covered path (Fig. 4a) and the positional error with respect to the goal (Fig. 4b). It is clear that the proposed algorithm (blue) traverses along a shorter trajectory as it will force the manipulator to stop moving after reaching the target position, while the artificial potential field (red) will not be able to bring the manipulator to a halt, as the robot fails to reach the goal. It is not surprising to observe that the proposed navigation algorithm is able to drive the positional error towards zero as it guides the tip towards the goal, while the artificial potential field fails to do so.

In the second scenario, we put the continuum manipulator in an environment consisting of several planar obstacles. The obstacles are placed at different heights to test whether the body of the manipulator is also able to avoid collisions with the obstacles while, at the same time, the tip is navigated towards the goal position. Fig. 5 shows the step-by-step

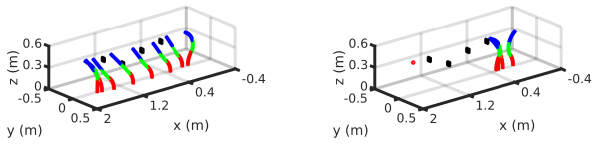

(a) (b)

Fig. 5. The scenario where the continuum manipulator is located at environment consisting of multiple static planar obstacles and the goal is shown as a red dot for (a) magnetic-field-inspired and (b) artificial potential field algorithm. The step-by-step configuration starts from the right to the left.

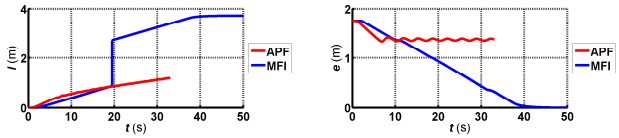

(a) (b)

Fig. 6. The plot of (a) the tip trajectory and (b) the position error for multiple obstacles for magnetic-field-inspired navigation (blue) and artificial potential field (red).

motion of the continuum manipulator using the magnetic-field-inspired (Fig. 5a) and artificial potential field (Fig. 5b) algorithms, respectively.

In Fig. 5a, we can observe that the magnetic-field-inspired navigation is able to guide the tip of the continuum robot towards the goal (red dot) while also ensuring that the body of the manipulator does not collide with the obstacles. Just like the tip's avoidance term, the body avoidance term works by appropriately moving the manipulator body sideways so that the manipulator does not get stuck in a local minimum. We can also observe how the redundancy mechanism employed helps to ensure that the body movement in avoiding obstacle does not disturb the movement of the manipulator's tip. The constraint avoidance, employed as a part of the redundancy control, also ensures that the manipulator's actuator variables do not get stretched more than the actuators' capability. This is in part also influenced by the use of geometric control and the property of the proposed vector field which keeps the tip at a constant speed during most of its motion.

In contrast, the artificial potential field applied to the tip and the body of the manipulator causes the manipulator to be trapped in a local minimum configuration as shown in Fig. 5b. This can also be observed in Fig. 6, where we can see that the proposed navigation (blue) is able to guide the tip to the goal with zero position error (Fig. 6b) despite longer path (Fig. 6a) compared to the artificial potential field (red).

B. Experimental Results

For the experimental scenario, a two-segment soft continuum manipulator prototype is used to validate the performance of the proposed algorithm. The manipulator consists of a hollow cylinder made of Ecoflex 00-50 Silicone. Each segment of the manipulator is 47 mm in length with an outer diameter of 23 mm and an inner diameter of 9 mm. Three pairs of pneumatically actuated pressure chambers (4.5

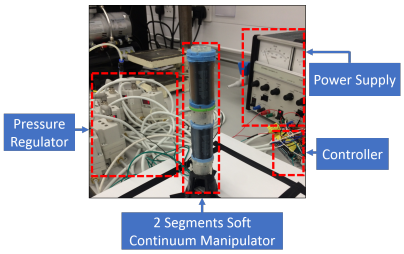

Fig. 7. The experimental setup depicts the 2 segments soft continuum robot actuated by pressure regulators.

Fig. 8. The experiment shows the 2-segments soft continuum manipulator avoids a simulated plane obstacle (black) using magnetic-field-inspired navigation.

mm diameter) are accommodated longitudinally in the wall. Each pair of chambers is connected to one inlet air pipe receiving regulated air pressure from a pressure regulator. The experimental setup is shown in Fig. 7. A single plane obstacle is simulated to be located in the surrounding space. Although the obstacle is simulated, its closest point is not known to the robot before it is closer to the obstacle than limit distance r_{l2}. Since we only employ two segments, we don't use the complete redundancy control in (24), but only the tip navigation term $\dot{\mathbf{q}}_t$.

In Fig. 8, we can see how the magnetic-field-inspired navigation is able to guide the tip of the 2-segment continuum manipulator avoiding the simulated plane obstacle drawn in black. Hence, we can see that the proposed navigation has a reactive property, i.e. it works without any prior information of the environment and relies only on a local information acquired online during the robot's movement. This demonstrates the potential of the method to be used for continuum manipulators operating in difficult scenarios involving not only unknown but also dynamic environments.

VI. CONCLUSIONS

In this paper, a reactive magnetic-field-inspired navigation is presented to guide the movement of a continuum manipulator towards the goal without colliding with unknown convex-shaped obstacles. The proposed navigation strategy is implemented in a modal-kinematics model of multi-segment continuum manipulators. A 2-segment soft continuum manipulator platform is used to validate the performance of the algorithm in a real-world scenario. The results show that the algorithm is able to outperform potential field algorithm in several scenarios repeatedly suffering from local minima. It is noted that, in achieving this performance, the proposed navigation only makes use of local information acquired during robot motion. In the future, the practical implementation of the algorithm in more difficult environments, consisting of non-convex, cluttered, and even dynamic environments will be explored. The use of a dynamic model of a continuum manipulator will also be investigated.

REFERENCES

[1] J. Fras, J. Czarnowski, M. Macias, J. Glowka, M. Cianchetti, and A. Menciassi, "New STIFF-FLOP module construction idea for improved actuation and sensing," in *Proc. IEEE Int. Conf. Robot. Autom.*, May 2015, pp. 2901–2906.

[2] P. Qi, C. Qiu, H. Liu, J. Dai, L. Seneviratne, and K. Althoefer, "A novel continuum-style robot with multilayer compliant modules," in *Proc. IEEE/RSJ Int. Conf. Intell. Robots Syst.*, Sep. 2014, pp. 3175–3180.

[3] F. Maghooa, A. Stilli, Y. Noh, K. Althoefer, and H. Wurdemann, "Tendon and pressure actuation for a bio-inspired manipulator based on an antagonistic principle," in *Robot. and Autom. (ICRA), 2015 IEEE Int. Conf. on*, May 2015, pp. 2556–2561.

[4] J. Granna, I. S. Godage, R. Wirz, K. D. Weaver, R. J. Webster, and J. Burgner-Kahrs, "A 3-D Volume Coverage Path Planning Algorithm With Application to Intracerebral Hemorrhage Evacuation," *IEEE Robotics and Automation Letters*, vol. 1, no. 2, pp. 876–883, Jul. 2016.

[5] M. Neumann and J. Burgner-Kahrs, "Considerations for follow-the-leader motion of extensible tendon-driven continuum robots," in *2016 IEEE International Conference on Robotics and Automation (ICRA)*, May 2016, pp. 917–923.

[6] C. Bergeles and P. Dupont, "Planning stable paths for concentric tube robots," in *Proc. IEEE/RSJ Int. Conf. Intell. Robots Syst.*, Nov. 2013, pp. 3077–3082.

[7] K. Wu, L. Wu, and H. Ren, "Motion planning of continuum tubular robots based on centerlines extracted from statistical atlas," in *2015 IEEE/RSJ International Conference on Intelligent Robots and Systems (IROS)*, Sep. 2015, pp. 5512–5517.

[8] Y. Chen, W. Xu, Z. Li, S. Song, C. M. Lim, Y. Wang, and H. Ren, "Safety-Enhanced Motion Planning for Flexible Surgical Manipulator Using Neural Dynamics," *IEEE Transactions on Control Systems Technology*, vol. 25, no. 5, pp. 1711–1723, Sep. 2017.

[9] H. Wang, J. Chen, H. Y. K. Lau, and H. Ren, "Motion Planning Based on Learning From Demonstration for Multiple-Segment Flexible Soft Robots Actuated by Electroactive Polymers," *IEEE Robotics and Automation Letters*, vol. 1, no. 1, pp. 391–398, Jan. 2016.

[10] J. Xiao and R. Vatcha, "Real-time adaptive motion planning for a continuum manipulator," in *Proc. IEEE/RSJ Int. Conf. Intell. Robots Syst.*, Oct. 2010, pp. 5919–5926.

[11] O. Khatib, "Real-time obstacle avoidance for manipulators and mobile robots," in *Proc. IEEE Int. Conf. Robot. Autom.*, vol. 2, Mar. 1985, pp. 500–505.

[12] A. Ataka, P. Qi, H. Liu, and K. Althoefer, "Real-Time Planner for Multi-Segment Continuum Manipulator in Dynamic Environments," in *Proc. IEEE Int. Conf. Robot. Autom.*, May 2016, pp. 4080–4085.

[13] L. Singh, J. Wen, and H. Stephanou, "Motion planning and dynamic control of a linked manipulator using modified magnetic fields," in *Proc. IEEE Int. Conf. Control Applicat.*, Oct. 1997, pp. 9–15.

[14] S. Haddadin, R. Belder, and A. Albu-Schffer, "Dynamic motion planning for robots in partially unknown environments," in *IFAC World Congr.*, vol. 18, 2011.

[15] J. D. Jackson, *Classical electrodynamics*, 3rd ed. New York, NY: Wiley, 1999. [Online]. Available: http://cdsweb.cern.ch/record/490457

[16] A. Ataka, H. K. Lam, and K. Althoefer, "Reactive Magnetic-field-inspired Navigation for Non-holonomic Mobile Robots in Unknown Environments," in *Proc. IEEE Int. Conf. Robot. Autom.*, May 2018, pp. 6983–6988.

[17] ——, "Reactive Magnetic-field-inspired Navigation Method for Robots in Unknown Convex 3d Environments," *IEEE Robotics and Automation Letters*, 2018, doi: 10.1109/LRA.2018.2853801.

[18] F. Bullo and R. M. Murray, "Proportional Derivative (PD) Control On The Euclidean Group," in *In European Control Conference*, 1995, pp. 1091–1097.

[19] I. S. Godage, G. A. Medrano-Cerda, D. T. Branson, E. Guglielmino, and D. G. Caldwell, "Modal kinematics for multisection continuum arms," *Bioinspiration & Biomimetics*, vol. 10, no. 3, p. 035002, 2015. [Online]. Available: http://stacks.iop.org/1748-3190/10/i=3/a=035002

[20] Y. Nakamura, H. Hanafusa, and T. Yoshikawa, "Task-Priority Based Redundancy Control of Robot Manipulators," *The International Journal of Robotics Research*, vol. 6, no. 2, pp. 3–15, 1987. [Online]. Available: https://doi.org/10.1177/027836498700600201